



# Self-assembly of semicrystalline PE-*b*-PS diblock copolymers within AAO nanoporous templates



María Teresa Casas<sup>a</sup>, Rose Mary Michell<sup>b</sup>, Iwona Blaszczyk-Lezak<sup>c</sup>, Jordi Puiggalí<sup>a</sup>,  
Carmen Mijangos<sup>c,d,e</sup>, Arnaldo T. Lorenzo<sup>b,f</sup>, Alejandro J. Müller<sup>b,d,e,\*</sup>

<sup>a</sup> Departament d'Enginyeria Química, Universitat Politècnica de Catalunya, Av. Diagonal 647, Barcelona E-08028, Spain

<sup>b</sup> Grupo de Polímeros USB, Departamento de Ciencia de los Materiales, Universidad Simón Bolívar, Apartado, 89000 Caracas 1080-A, Venezuela

<sup>c</sup> Instituto de Ciencia y Tecnología de Polímeros, CSIC, Juan de la Cierva, 3, 28006 Madrid, Spain

<sup>d</sup> POLYMAT and Polymer Science and Technology Department, Faculty of Chemistry, University of The Basque Country UPV/EHU, Paseo Manuel de Lardizabal 3, 20018 Donostia-San Sebastián, Spain

<sup>e</sup> IKERBASQUE, Basque Foundation for Science, Bilbao, Spain

<sup>f</sup> The DOW Chemical Company, 2301 N Brazosport Blvd., Freeport, TX 77541, USA

## ARTICLE INFO

### Article history:

Received 28 January 2015

Received in revised form

22 April 2015

Accepted 14 June 2015

Available online 24 June 2015

### Keywords:

Confined crystallization

Core-shell morphology

AAO templates

Block copolymers

## ABSTRACT

Strongly segregated polyethylene-*b*-polystyrene (PE-*b*-PS) diblock copolymers were infiltrated within anodic aluminum oxide nanoporous templates (AAO) (with 60 nm diameter). After carefully removing the nanofibers from the nanopores, TEM revealed their morphology. This is the first time that the morphology of semi-crystalline diblock copolymers infiltrated within AAO templates is observed. Regardless of their composition, the infiltrated nanofibers are constituted by core-shell or pseudo core-shell self-assembled nanocylinders. The affinity of PE to the AAO walls tailors the morphology towards PE shells with PS cores. The PS cores for some compositions have PE inclusions whose morphology is expected on the basis of previous computer simulation studies. Morphological observations successfully explain the confined crystallization of the PE block within the nanopores and the origin of novel double confinement effects (induced by glassy PS block and rigid AAO walls) on the PE block.

© 2015 Elsevier Ltd. All rights reserved.

## 1. Introduction

Confined crystallization within nano-structured materials has been extensively studied in the last decade [1–9]. Recently, polymer crystallization within inorganic templates, such as Anodic Aluminum oxide (AAO) templates, has been investigated. The interested reader is referred to two recent reviews and references there in [10,11]. In this hybrid nanoporous system, polymer crystallization occurs under confinement, in a similar way to other confined crystallization cases previously reported in the literature, such as in droplets, blends, block copolymers and nanolayers [1–11].

Microdomains (MDs) size (a term applied generically to the micron or nanometer scale in this paper) can determine the confined crystallization behavior, especially when MDs are truly

isolated [1–11]. In the case of crystallization within AAO nanopores, it has been reported that crystallization temperatures decrease with nanopore diameter. However, when the infiltrated material is a strongly segregated diblock copolymer, the size of the MDs within nanopores is determined by the composition of the block copolymer, the relationship between the size of the MDs in bulk and nanopore diameter, and also the affinity of the blocks with the AAO surface [12–19]. Hence, it is possible, by changing the block copolymer composition, to obtain different MDs sizes within the same AAO template.

Very few works have dealt with the study of the crystallization of infiltrated block copolymers within AAO nanoporous templates [20,21]. Strongly segregated linear diblock copolymers [2–10] undergo phase segregation according to their composition. The segregation strength is dictated by the product of the Flory–Huggins interaction parameter between the blocks and the degree of polymerization. Linear PE-*b*-PS diblock copolymers have been studied by us in the past [22–25]. These copolymers were synthesized by living anionic polymerization with narrow molecular weight distributions and chain lengths high enough to produce

\* Corresponding author. POLYMAT and Polymer Science and Technology Department, Faculty of Chemistry, University of The Basque Country UPV/EHU, Paseo Manuel de Lardizabal 3, 20018 Donostia-San Sebastián, Spain.

strong phase segregation. In the strong segregation regime, the PE block is forced to crystallize within the confined spaces dictated by the diblock copolymer phase segregated morphology upon cooling from the melt. The consequence of such confinement into lamellae, cylinders or spheres is a change in nucleation that produces fractionated crystallization. As confinement increases, surface nucleation becomes dominant for the PE blocks and the Avrami index decreases to values close to one [1–11,22–25].

Recently, Michell et al. [20] studied the crystallization of infiltrated PE-*b*-PS diblock copolymers into AAO templates. They obtained unexpected results indicating that the PE block experienced a novel double confinement effect once the copolymer was infiltrated in the cylindrical nanopores. It was speculated that both the vitreous PS block (covalently bonded to the PE block) and the AAO nanocavities were inducing two types of confinement in the PE block. The origins of the effect could not be precisely ascertained, since the changes of the copolymer morphology upon infiltration were unknown.

We study in this paper, for the first time, the morphology of PE-*b*-PS diblock copolymers infiltrated within AAO templates and its relationship with the crystallization behavior of the PE blocks. As far as the authors are aware, this is the first time that the morphology of infiltrated semi-crystalline diblock copolymers is revealed, since previous works have dealt with the morphology of infiltrated amorphous diblock copolymers [12–14]. The results obtained successfully explain the confined crystallization of the PE block within the self-assembled structure that results from infiltration in the nanopores. Additionally, the origin of the novel double confinement effect that was previously reported by us [20] is explained once the morphology of the infiltrated copolymer is visualized.

## 2. Experimental

The precursors of the materials employed were poly(1,4-butadiene)-*block*-polystyrene diblock copolymers (PB-*b*-PS). The synthesis of these materials was reported previously [22]. It was performed by sequential anionic polymerization of butadiene and styrene. These precursors were later hydrogenated in order to obtain PE-*b*-PS linear diblock copolymers.

Table 1 reports the molecular characteristics of the materials employed for infiltration (branch content and polydispersity index, PDI). The superscripts indicate the number average molecular weight ( $M_n$ ) and the subscripts the composition in weight %. The molecular weight of the PE block is constant in all the samples employed.

Ordered AAO templates were prepared by two-step electrochemical anodization of aluminum [26,27]. The infiltration of the block copolymers into alumina templates with 60 nm diameter pores (see Fig. 1) was carried out by placing the solid materials on top of the AAO template at 170 °C and then annealing them at 180 °C, under a nitrogen atmosphere for 5 h.

The bulk morphology of the PE-*b*-PS diblock copolymers was examined by bright field TEM using a JEOL 1220 operated at 100 kV. Thin sections were cut at –130 °C using an LEICA EMFCS ultra-cryomicrotome equipped with a diamond knife. The samples were stained by exposure to RuO<sub>4</sub> vapor.

On the other hand, the infiltrated samples were extracted from the AAO templates using 5% NaOH w/v in a water/methanol solution. Samples were immersed for only 90 min in order to get a partial dissolution of AAO. This allowed the observation of the nanofiber aggregates and also the possibility of obtaining a sufficiently soft sample for being subsequently cut. The solvent treatment applied to dissolve the AAO templates did not affect the infiltrated fibers. There were two evidences that indicate they were

**Table 1**  
Molecular characteristics of the samples.

Sample	% 1,2 Units	$M_n$ (kg/mol) (PE block)	PDI
PE <sub>25</sub>	11.0	24.4	1.01
E <sub>79</sub> S <sub>21</sub> <sup>51</sup>	12.6	31.0	1.02
E <sub>53</sub> S <sub>47</sub> <sup>51</sup>	11.3	26.4	1.04
E <sub>26</sub> S <sub>74</sub> <sup>105</sup>	11.3	26.4	1.05
E <sub>11</sub> S <sub>89</sub> <sup>244</sup>	11.3	27.6	1.02

not affected: (a) their diameters and exact shape corresponded with the template nanopores (see results section) and (b) we performed blank tests where PE/PS were exposed to the same 5% NaOH w/v in a water/methanol mixture and then observed their surfaces by SEM and no attack on the samples was appreciated (see images in the [Supplementary Material](#)).

The extracted nanofibers were stained with RuO<sub>4</sub> vapor during three days. Samples were embedded in Spurr resin and cut with a diamond knife and later deposited onto carbon-coated copper grids. Finally the samples were observed in a TEM FEI Tecnai 10, operated at 100 KV. Bright field micrographs were taken with a Mega View 3 digital camera from Olympus Soft Imaging Solutions. Fig. 2 shows a schematic of the procedure involved in sample preparation.

A DSC Pyris Perkin Elmer instrument, calibrated with tin and indium under an ultra high purity nitrogen atmosphere, was employed to study the thermal properties of the materials. Cooling and heating rates of 30 °C/min were employed. For the infiltrated samples, the total mass (block copolymer plus AAO template) was 25 mg, while the block copolymer mass was approximately 0.5 mg according to TGA experiments. The results were compared with those obtained with PE-*b*-PS neat samples at the same scanning rates and employing a mass of 2 mg.

## 3. Results and discussion

Fig. 3 shows representative micrographs of the different morphologies adopted by the PE-*b*-PS diblock copolymers. The block copolymers employed for infiltration have been the subject of previous studies [22–25]. The morphology of infiltrated semi-crystalline copolymers has never been reported before. Since a dramatic change in morphology occurred upon infiltration, the morphology of the bulk samples (before infiltration) is also included in Fig. 3 for comparison purposes.

In the case of bulk un-infiltrated copolymers, Fig. 3 shows the typical composition dependent morphologies exhibited by strongly segregated PE-*b*-PS diblock copolymers [22]. As the PE content in the copolymers decreases from 79 to 11%, the following morphologies can be clearly distinguished (PS block MDs appear dark gray in the micrographs, while PE block MDs appear light gray): PS spheres/PE matrix (with full percolation of the PE matrix), PS/PE lamellae (with percolation paths between MDs caused by defects in the lamellar morphology), PE cylinders/PS matrix (where cylinders are generally isolated, although percolation between them is also possible) and finally PE spheres/PS matrix (where most spheres are isolated within the glassy PS matrix). Table 2 shows the sizes of the PE block MDs obtained previously by SAXS and TEM [22]. For more details on the bulk morphology of the copolymers, see reference [22].

The infiltration process leads to a large reorganization of the diblock copolymer MDs. Fig. 3 summarizes the morphological changes. The structures observed by TEM are within groups of fibrils extracted from the AAO template that have been embedded in

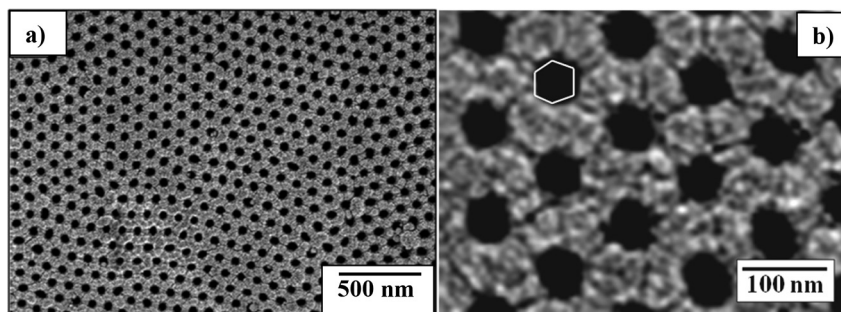


Fig. 1. Top view of an AAO template with 60 nm pore diameter.

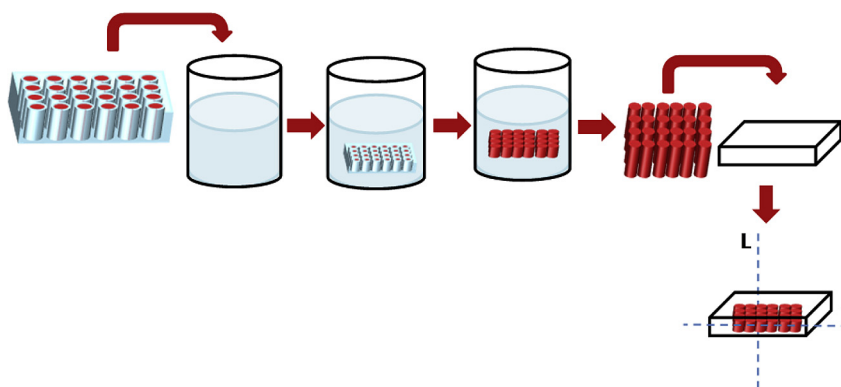


Fig. 2. Schematic representation of the experimental procedure for the preparation of the samples observed by TEM. The AAO templates were dissolved to extract the nanofibers within them. Nanofibers aggregates were then embedded in spurr resin. T and L represent the lines along which transversal and longitudinal cuts were made to the embedded samples.

spurr resin to facilitate their sectioning and observation (see Fig. 2). Additional images have been included in the Supplementary Material.

The embedded nanofibers aggregates were ultra-cryo-microtomed into thin sections that were cut parallel to the fiber axis (labeled “Longitudinal” in Fig. 3) and perpendicular to it (“Transversal” in Fig. 3). Fig. 2 also indicates how these longitudinal and transversal cuts were made. In some cases, it is possible to observe small distortions originated by sample preparation. In order to facilitate the visualization of the structures obtained, the boundaries between fibrils (i.e., fibrils outer edges) are depicted with dashed lines in representative parts of the micrographs of Fig. 3.

For a clear understanding of the morphologies presented in Fig. 3, Fig. 4 shows a schematic representation of the blocks distribution inside the nanopores of the AAO template based on extensive TEM observations.

The nanopores are not really perfectly cylindrical but have an approximate hexagonal shape, as apparent in Figs. 1 and 3 and schematically depicted in the outer shape of the aggregated nanofibers in Fig. 4 (where hexagonal cross-sections has been depicted in the top views). The templates are first prepared with 35 nm pores (that have a more regular cylindrical shape), but are later enlarged until the desired 60 nm size is obtained. During this enlargement process achieved by treatment in phosphoric acid (5%  $\text{H}_3\text{PO}_4$ ) at 35° C during 25 min, the pores change to their final hexagonal like shapes. As a result, the extracted nanofibers also have hexagonal-like outer surfaces that can be seen when a whole aggregated group of them has been embedded in spurr and cut together (see Fig. 1 through 4).

In general, core–shell structures (or pseudo core–shell, where the shell is clear but the core may also contain some of the shell

material dispersed in it) are seen in Fig. 3 (see also Fig. 4) for all samples, regardless of the original morphology in the bulk.

The final morphology of a block copolymer within AAO templates depends on its composition, but also on the following two aspects [12–19]: (a) the relationship between the size of the MDs and the inter-domain distances in the bulk and the diameter of the AAO nanopores and (b) the preferential affinity of one block to the AAO wall.

Taken into account the above and the micrographs in Fig. 3 (see the “transversal” micrographs and also the schematic representation in Fig. 4), it is evident that the PE block has a stronger affinity to the AAO surface as compared to the PS block, since it always appears at the outer part of the fibers (i.e., shells). This probably stems from its apolar nature. Fig. 3 shows that the PE block always forms the shell while PS constitutes the core of the observed core–shell nanocylinders.

In some cases, the composition of the core is more complex (see below). Even when the PE content in the diblock is only 11%, the PE block is situated between the AAO wall and the PS block. The affinity between PE and the AAO nanopore walls dictates in this case the morphology. The composition regulates, as expected, the relative sizes of the core (and its inner morphology) and shell of the concentric nanocylinders generated inside the templates.

In the transversal cut shown in Fig. 3 (and Fig. 4), it is possible to observe the distribution of the blocks inside the pores looking down from the top of the template. In the boundary between PE and PS blocks (see Fig. 3), a dark shade that corresponds to the amorphous interphase between the blocks is observed. The interphase is stained during sample preparation. The same dark shade can be observed between the blocks in the un-infiltrated case [22].

The inner cylinders correspond to PS blocks in the core–shell morphologies and they exhibit irregularities in some cases,



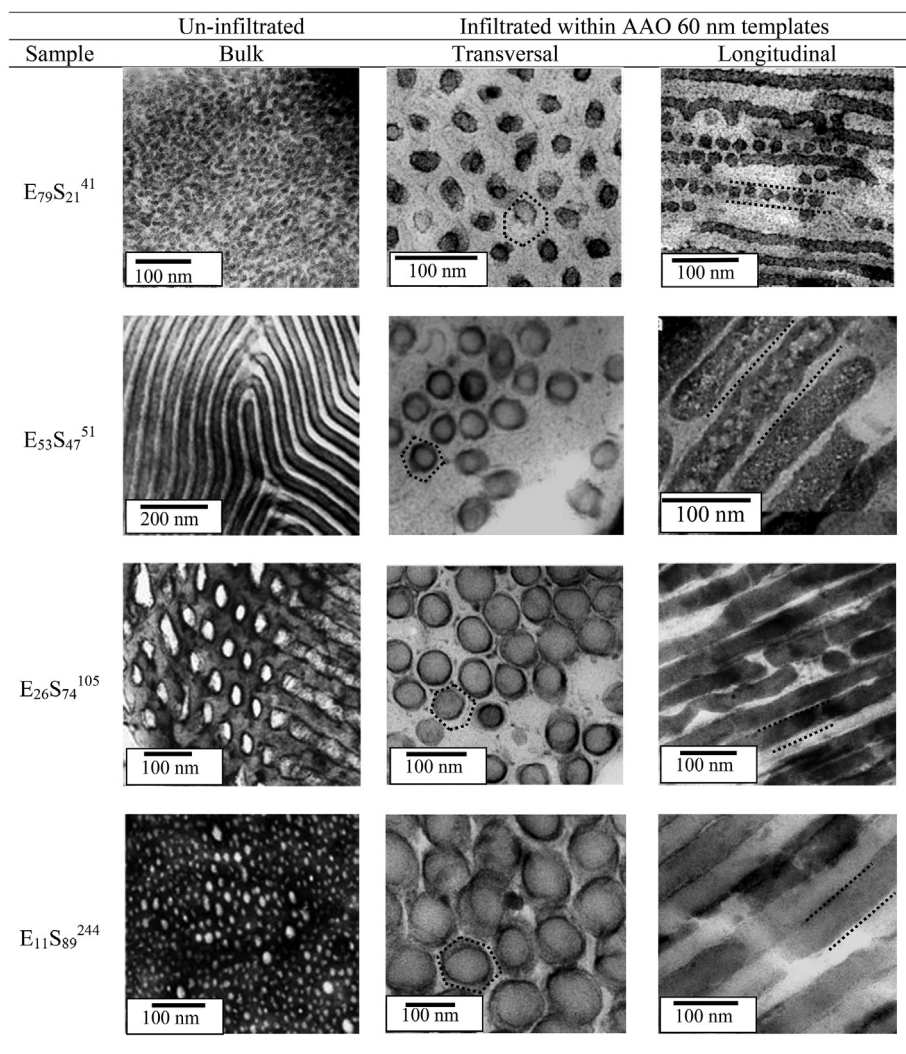


Fig. 3. PE-*b*-PS diblock copolymer morphologies before and after infiltration within AAO templates as revealed by TEM.

especially in the infiltrated  $E_{79}S_{21}^{41}$  sample. For this copolymer, PS is the minor component, and the longitudinal cut reveals that the MDs exhibit a transition between cylinders and spheres (see Figs. 3 and 4). Yu et al. [17] studied the possible morphologies of a copolymer with an asymmetrical composition forming hexagonally packed cylinders in the bulk. Their predictions are based on computer simulations of a lattice model by applying simulated annealing. Their simulations indicate that [17] when the majority

block (i.e., PE) is attracted to the wall, and the diameter of the nanopore in the AAO template is small with respect to the inter-domain distance of the minority block (i.e., PS) in the bulk, both cylinders and spheres of the minority block may be observed. Hence the present results for the infiltrated  $E_{79}S_{21}^{41}$  morphologies are in agreement with their theoretical prediction.

In the case of a symmetrical diblock copolymer, the results of both simulations and experiments (for amorphous diblock copolymer samples) indicate that concentric cylinders are the most common morphology after infiltration. According to Monte Carlo simulations performed by Wang [16], a lamellar diblock copolymer should change its morphology after infiltration to a concentric cylindrical morphology, where the number of cylinders depends on the template pore diameter. An interesting feature is that this prediction establishes the possibility of a transitional morphology, where a clear core may not be observed. These predictions could partially explain the morphology observed in the infiltrated block copolymer  $E_{53}S_{47}^{51}$ . In this block copolymer, the PS core contains inclusions of the PE block, while the rest of the PE block still forms the shell attached to the AAO walls (see Figs. 3 and 4).

On the other hand, Sevink and Zvelindovsky [15] employed dynamic density functional theory, in order to predict infiltrated block copolymer morphologies. They found a large variety of

**Table 2**  
Domain Size “*l*” and spacing “*d*” of the PE-*b*-PS diblock copolymers as determined by TEM and SAXS measurements at room temperature [22].

Sample	TEM		SAXS	
	<i>l</i> (nm)	<i>d</i> (nm)	<i>d</i> (nm)	Bulk Morphology
PE <sup>25</sup>	—	—	—	Bulk
$E_{79}S_{21}^{41}$	—	—	—	PS cylinders in a PE matrix
$E_{53}S_{47}^{51}$	$16^a \pm 3$	$62^c \pm 3$	65	Lamellae
$E_{26}S_{74}^{105}$	$21^b \pm 5$	$126^c \pm 29$	99	PE Cylinders
$E_{11}S_{89}^{244}$	$12^b \pm 2$	$105^c \pm 13$	108	PE Spheres

<sup>a</sup> Thickness of the PE lamellae.

<sup>b</sup> Radius of the microdomain.

<sup>c</sup> Interdomain distance.

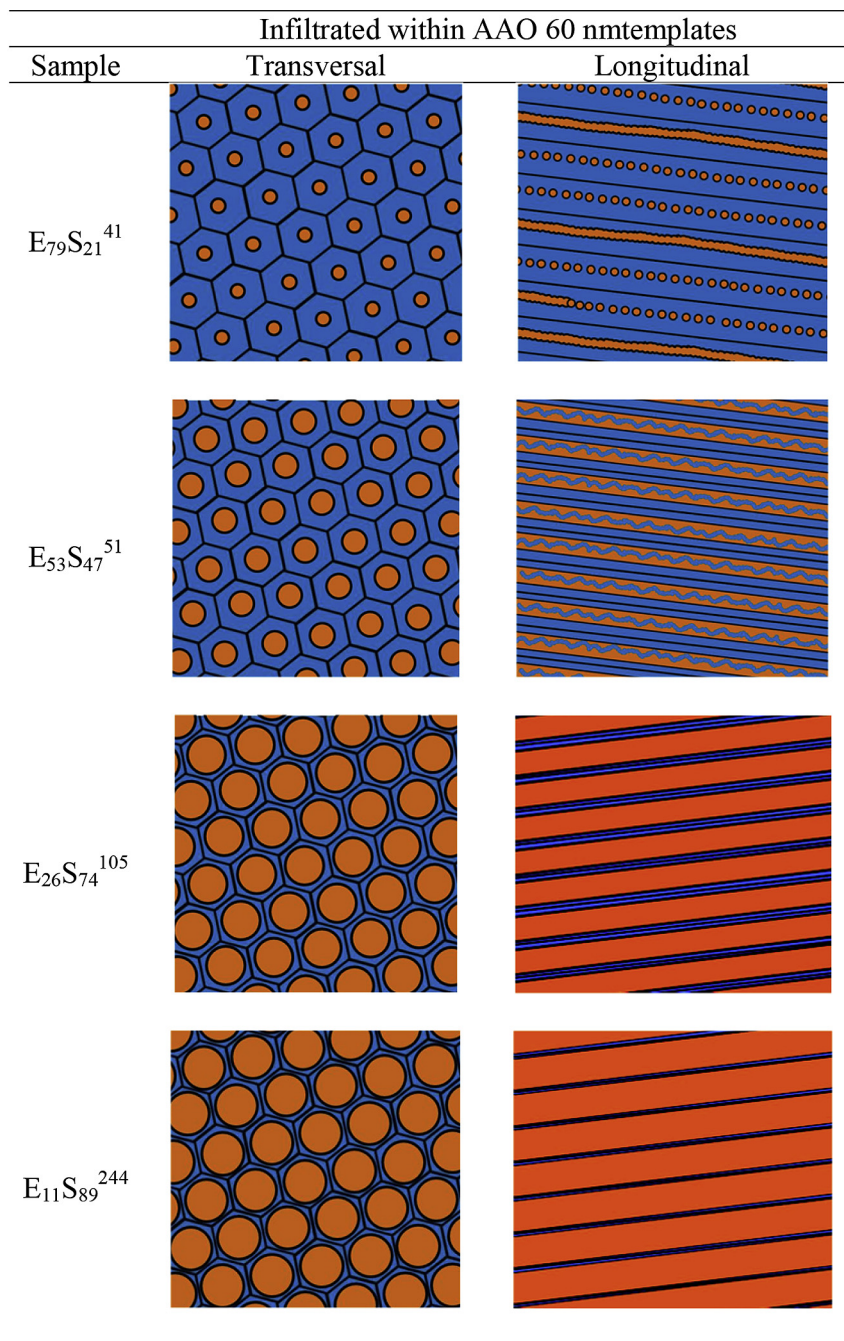


**Fig. 4.** Schematic representation of the morphologies observed by TEM in Fig. 3 corresponding to the infiltrated PE-*b*-PS diblock copolymer within AAO templates. PE blocks are shown in blue and PS blocks in orange. (For interpretation of the references to color in this figure legend, the reader is referred to the web version of this article.)

possible structures, including a helical conformation, that is consistent with the morphology of the inclusions observed for the core in  $E_{53}S_{47}^{51}$ . Considering this prediction and the experimental observation (see Fig. 3) we conclude that the PE block is in the external border of the fibril (due to its affinity to the AAO wall), but also has a helical conformation in the inclusions within the center of the PS cores (see Figs. 3 and 4).

In the case of the  $E_{26}S_{74}^{105}$ , the observed morphology after infiltration is the expected by Yu et al. [17] for a system with a small pore diameter when the minor block has a preference for the AAO wall. In those cases, Yu et al. [17] predicted a core shell morphology with the minor block forming the shell and the major block the

core. Figs. 3 and 4 show that  $E_{26}S_{74}^{105}$  exhibits a morphology that fits perfectly with that predicted by Yu et al. [17].

For the copolymer with only 11% PE, the morphology changed from PE nanospheres in the bulk sample to core-shell cylinders after infiltration, where the PE block forms the shell attached to the AAO walls. Drobiyal et al. [12] reported for infiltrated polystyrene-*block*-polybutadiene diblock copolymers (PS-*b*-PB) with spherical MDs in the bulk, different morphologies depending on the nanopore diameter. When the nanopore diameter was small, a morphology similar to the one reported here for  $E_{11}S_{89}^{244}$  was observed, however when the diameter of the pores was larger than a critical value, the authors reported a spherical morphology inside the nanopores.

Table 3 presents estimated values of the PS core diameters ( $\phi_{theo}$ ) calculated by assuming that perfect core–shell cylinders (with circular cross-sections) are formed (filling the 60 nm pores). It was also considered that the inner and outer diameters have values proportional to the block copolymer composition. Then, the PS core diameters were experimentally determined ( $\phi_{exp}$ ) by measuring them directly on the TEM micrographs (assuming circular cross-sections). The experimentally determined values are a perfect match to the theoretical expectations based on copolymer composition, when the core–shell morphology is not distorted (i.e., for  $E_{26}S_{74}^{105}$  and  $E_{11}S_{89}^{244}$ ). In the cases where the PS core is distorted or contains PE block inclusions the correlation between the experimental value and theoretical estimation is not as good, as expected.

Table 3 also lists the extended chain length value of the PE and PS chains within each block (calculated from the number average molecular weight values). For the PS case, the unperturbed average end to end distance of the chains was also calculated ( $\langle r_0^2 \rangle^{1/2}$ ). The chain dimensions can perfectly fit within the AAO nanopores and can generally form the observed morphologies without significant conformational changes (in the case of the PS cores). For the case of the PS block within the  $E_{79}S_{21}^{41}$  diblock copolymer, the small chain length probably contributes to the morphological instability observed in Fig. 3 (cylinders and spheres).

Fig. 5 shows DSC cooling scans from the melt (after thermal history was erased) for PE and PE-*b*-PS diblock copolymer samples, before and after infiltration within AAO templates. It is important to note that the molecular weight and branch content of neat PE and the PE block within the copolymers are constant for all the samples studied here [22]. Therefore, any changes observed in the crystallization behavior are a consequence of the confinement of PE chains.

Neat PE exhibits a sharp crystallization exotherm at 85 °C originated by heterogeneous nucleation (labeled  $\alpha$  exotherm) where most of the sample crystallizes upon cooling from the melt (Fig. 5a). Additionally, it displays a very small exotherm at much lower temperatures (i.e., 52 °C) which is due to intramolecular fractionation (labeled IF), a process typical of branched polyethylene samples [28].

In the un-infiltrated diblock copolymer cases, a fractionated crystallization of the confined PE block (cylinders and spheres) can be observed in Fig. 5 for  $E_{26}S_{74}^{105}$  and  $E_{11}S_{89}^{244}$  (that has been studied previously for these block copolymers (see refs. 22–25 for a detailed explanation of the DSC results and fractionated crystallization). Fractionated crystallization occurs when the number of MDs is in the same order of magnitude than the number of the most active heterogeneities present in the bulk polymer under consideration. The most active heterogeneities are capable of producing nucleation at low supercooling and generate the high temperature  $\alpha$  crystallization exotherms. The crystallization of the PE block is fractionated into several exotherms, labeled in decreasing temperature order as  $\alpha$ ,  $\beta$  and  $\gamma$ . Exotherm  $\beta$  is also generated by

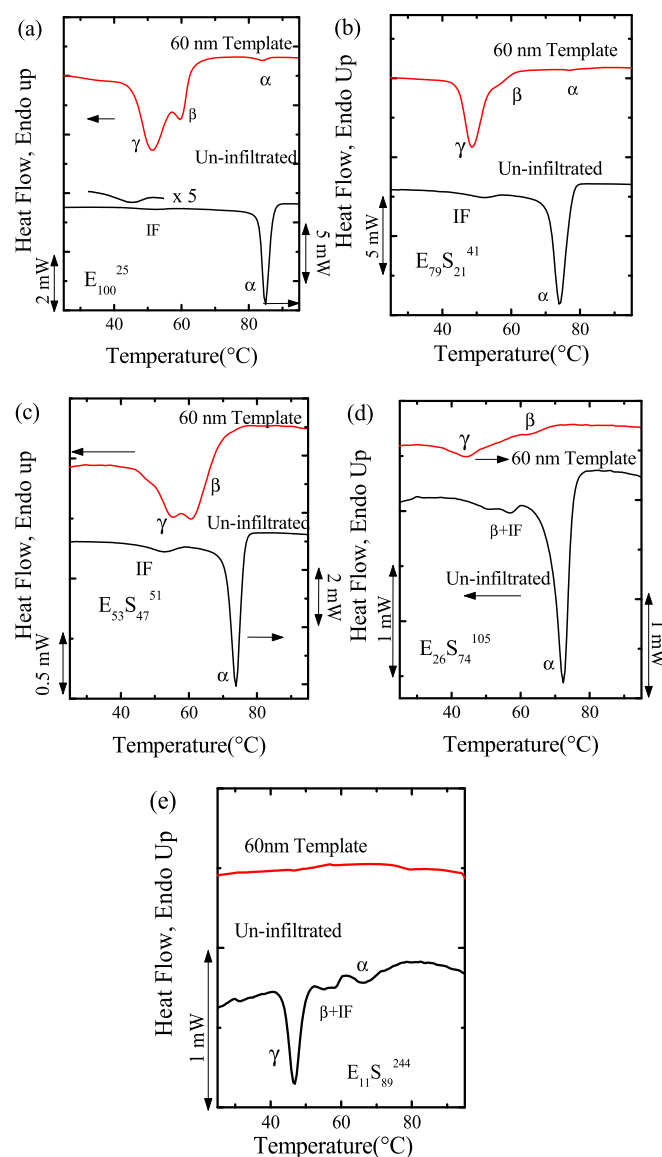


Fig. 5. DSC cooling scans at 30 °C/min for the indicated samples before and after infiltration within AAO 60 nm templates [20].

heterogeneous nucleation, but with less active heterogeneities than those nucleating the  $\alpha$  process (see Refs. [22–25]).

Exotherm  $\gamma$  is due to the crystallization of clean MDs that do not possess heterogeneities within them.  $E_{11}S_{89}^{244}$  is the only un-infiltrated copolymer that crystallizes predominantly in the  $\gamma$  exotherm (Fig. 5e). This is a consequence of the unlikely percolation or

Table 3

Extended chain length ( $L$ ) for each block, PS block core diameter (after infiltration), root mean square value of the unperturbed end to end distance of the PS block.

	$M_{PE}$ (kg/mol)	$M_{PS}$ (kg/mol)	PE block	PS block			$\langle l_0^2 \rangle^{1/2}$ (nm)
			$l_{PE}$ (nm)	$l_{PS}$	$\phi_{theo}$	$\phi_{exp}^a$	
				(nm)	(nm)	(nm)	
$E_{79}S_{21}^{41}$	32.4	8.6	291	21	13	$26 \pm 4$	6.2
$E_{53}S_{47}^{51}$	27.0	24.0	243	58	28	$40 \pm 4^b$	10.4
$E_{26}S_{74}^{105}$	27.3	77.7	245	188	44	$44 \pm 4$	18.7
$E_{11}S_{89}^{244}$	26.8	217.2	241	525	53	$52 \pm 4$	31.2

<sup>a</sup> Measured from the TEM micrographs.

<sup>b</sup> Overestimated value because the PS core contains PE block helical inclusions.



interconnection between isolated PE spheres. Additionally, in this case, the number of clean MDs (PE nanospheres) is six orders of magnitude larger than the number of heterogeneities in bulk PE [29].

The crystallization of the PE block isolated MDs that occur in the  $\gamma$  exotherms can start from homogeneous nuclei or from surface nucleation. Our previous works concluded that the PE block crystallizes by surface nucleation (at the interphase between the PE and the PS block) because crystallization does not occur at extreme supercoolings ( $T_c$  is still far from  $T_g$ ). In fact, in our opinion, homogeneous nucleation has never been seen in PE, in spite of claims to the contrary (extensive discussion on this topic can be found in references 2,7,10,11) [2,6,7].

When the diblock copolymers are infiltrated (as well as neat PE) into the AAO templates, the crystallization occurs mostly at low temperatures in  $\gamma$  exotherms, while the  $\beta$  and  $\alpha$  exotherms become very small. The number of nanopores in the templates (of the order of  $10^{12}/\text{cm}^3$ ) exceeds in three orders of magnitude the number heterogeneities typically present in PE (of the order of  $10^9/\text{cm}^3$ , see ref. 29). Therefore, statistically speaking if there is no remaining film on top of the template that can interconnect nanopores (and cause percolation through which crystallization can spread), the crystallization occurs in mostly heterogeneity free isolated cavities.

Fig. 6 illustrates the general decrease in crystallization temperatures observed after infiltration as a consequence of confinement in AAO nanopores. Lines joining the experimental data points corresponding to the dominating crystallization temperatures (i.e., whose peak  $T_c$  values correspond to the largest enthalpy exotherms) are drawn in Fig. 6.

A particularly interesting case is  $E_{26}S_{74}^{105}$ . In this diblock copolymer in the bulk, the PE block forms cylinders (Fig. 3) that exhibit some percolation that is responsible for the appearance of the fractionated crystallization [22]. The crystallization of isolated heterogeneity free cylinders occurs at 50 °C (corresponding to the  $\gamma$  exotherm in Fig. 5d). When this sample is infiltrated in the 60 nm nanopores, the crystallization temperature corresponding to the  $\gamma$  exotherm is depressed to lower temperatures (see Figs. 5d and 6) giving rise to a novel “double confinement” effect [20]. However, when this effect was recently reported [20], the morphological change experienced by the sample upon infiltration was unknown.

Thanks to the TEM experiments performed here (Fig. 3), the origin of double confinement in the PE nanocylinders of  $E_{26}S_{74}^{105}$  can

now be finally established. The PE block phase is confined at two different surfaces (thereby originating two types of confinement or double confinement):

(a) the interface between the alumina and the PE shell

and

(b) the interphase between the PE shell and the covalently linked glassy PS core.

If the morphology was different, for instance a PE core with a PS shell in contact with alumina walls, the double confinement would not exist and there would be no difference in crystallization behavior between un-infiltrated and infiltrated copolymer. Therefore, the observation of the morphology of the nanofibers is essential to correctly interpret the changes in crystallization behavior due to infiltration into AAO templates.

As was pointed out by Carvalho and Dalnoki-Veress [30,31] the nature of the surface has an important influence in the crystallization temperature of isolated MDs. They demonstrated that in the case of well dispersed heterogeneity free polyethylene droplets, the crystallization occurred preferentially at the surface of the droplets and never inside their volume. Hence surface nucleation is the dominant mechanism in the PE case, instead of homogeneous nucleation (which would occur within the droplets volume).

Table 4 shows estimated values of the volume corresponding to PE MDs for selected samples and their corresponding  $\gamma$  peak temperatures. The volumes were estimated by measuring the size of the PE shells in the micrographs of Fig. 3 and the knowledge of the lengths of the nanopores (i.e., 100  $\mu\text{m}$ ), always assuming that the shapes were always perfect concentric cylinders.

Table 4 shows for the infiltrated samples a correlation between  $T_c$  and volume, since in most cases, a reduction in volume leads to a reduction in crystallization temperature. In the particular case of the  $E_{53}S_{47}^{51}$  diblock copolymer the volume is underestimated, due to a limitation to exactly estimate the volume of the PE inclusions inside the PS core.

The volume of the PE MDs for neat  $E_{11}S_{89}^{244}$  was calculated in order to establish the importance of the surface nature during PE crystallization. In this case, the results presented in Table 4 show no correlation between the volume of the PE phase and the crystallization temperature in comparison to the infiltrated samples. The volume of the PE spheres is 5 orders of magnitude smaller than the volume of any of the infiltrated PE block MDs, and the crystallization temperature is similar in both cases. Such lack of overall dependence of  $T_c$  on the volume of the MDs (with different surfaces or interphases), indicate that the nucleation is not homogeneous and depends on the exact nature of the surface or interphase (e.g., alumina versus glassy PS). For homogeneous nucleation, a clear

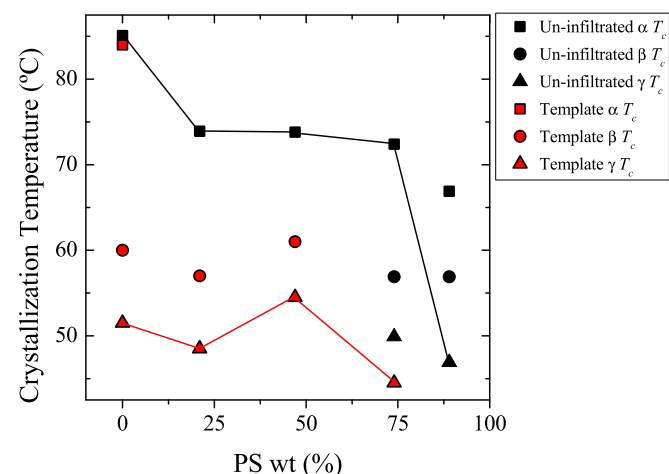


Fig. 6. Peak crystallization temperatures obtained from Fig. 5. The solid lines join the data points where the dominant crystallization peak of each sample was found (i.e., largest latent crystallization enthalpy exothermic peaks). Red symbols are for infiltrated materials and black symbols for bulk samples. (For interpretation of the references to colour in this figure legend, the reader is referred to the web version of this article.)

Table 4  
Estimated volume of PE MDs for selected samples.

Sample	V (nm <sup>3</sup> )	T <sub>c</sub> (°C)
PE/35 nm AAO <sup>a</sup>	9.62 × 10 <sup>7</sup>	45.1
PE/60 nm AAO	2.83 × 10 <sup>8</sup>	51.5
E <sub>79</sub> S <sub>21</sub> <sup>41</sup> /60 nm AAO	1.83 × 10 <sup>8</sup>	48.5
E <sub>53</sub> S <sub>47</sub> <sup>51</sup> /60 nm AAO	1.74 × 10 <sup>8b</sup>	54.5
E <sub>26</sub> S <sub>74</sub> <sup>105</sup> /60 nm AAO	1.08 × 10 <sup>8</sup>	44.5
E <sub>11</sub> S <sub>89</sub> <sup>244</sup> /60 nm AAO	5.06 × 10 <sup>7</sup>	—
E <sub>11</sub> S <sub>89</sub> <sup>244</sup> in bulk	7.24 × 10 <sup>3c</sup>	46.9

<sup>a</sup> From ref [11].

<sup>b</sup> Underestimated, since the volume calculated corresponds only to the external shell (and in this case there are PE helical inclusions within the PS cores).

<sup>c</sup> Calculated as the volume of a sphere with a diameter of 24 nm.

correlation with the phase volume would have been expected [2,30,31].

The infiltration of  $E_{11}S_{89}^{244}$  within the 60 nm template leads to an undetected level of crystallization in the infiltrated material (Fig. 4e). This is probably due to the presence of a small amount of crystals in the sample, which resulted in an extremely low value of exothermic heat that was not detected by our DSC.

#### 4. Conclusions

The morphology of a semi-crystalline diblock copolymer infiltrated within AAO templates was observed for the first time. The morphologies obtained allow us to explain the changes of the crystallizing phase upon infiltration. The origin of the novel double confinement effect, recently reported by some of us, has been satisfactorily explained by the observed core–shell morphologies, where the PE block was found to form the shell in contact with the alumina walls, while the PS constituted the core of the nanofibers. The sizes of the MDs and their exact morphology (since they can contain inclusions or imperfections) are determined by block copolymer composition but the overall core–shell shape are dictated by the affinity of the PE block towards the alumina walls. The PE phase was found to experience surface nucleation either at the alumina walls or at the PE-*b*-PS diblock copolymer interphase.

#### Acknowledgments

We gratefully acknowledge the contribution of Adriana Boschetti de Fierro and Volker Abetz in the block copolymer synthesis reported in previous works [22–25].

The POLYMAT/UPV/EHU team would like to acknowledge funding from the following projects: “UPV/EHU Infrastructure: INF 14/38”; “Mineco/FEDER: SINF 130I001726XV1/Ref: UNPV13–4E–1726” and “Mineco MAT2014-53437-C2-P”.

#### Appendix A. Supplementary data

Supplementary data related to this article can be found at <http://dx.doi.org/10.1016/j.polymer.2015.06.025>.

#### References

- [1] H. Frensch, P. Harnischfeger, B.J. Jungnickel, Fractionated crystallization in incompatible polymer blends, in: L.A. Utracki, R.A. Weiss (Eds.), *Multiphase Polymers: Blends and Ionomers* ACS Symposium Series 395, American Chemical Society, Washington, 1989, pp. 101–125.
- [2] A.J. Müller, V. Balsamo, M.L. Arnal, *Adv. Polym. Sci.* 190 (2005) 1–63.
- [3] I.W. Hamley, *Adv. Polym. Sci.* 148 (1999) 113–137.
- [4] Y. Loo, A. Register, Crystallization within block copolymer mesophases, in: I.W. Hamley (Ed.), *Developments in Block Copolymer Science and Technology*, Wiley, New York, 2004.
- [5] R.V. Castillo, A.J. Müller, *Prog. Polym. Sci.* 34 (2009) 519–560.
- [6] A.J. Müller, V. Balsamo, M.L. Arnal, Crystallization in block copolymers with more than one crystallizable block, in: G. Reiter, G. Strobl (Eds.), *Lecture Notes in Physics: Progress in Understanding of Polymer Crystallization*, vol. 714, Springer, Berlin, 2007, pp. 229–259.
- [7] A.J. Müller, M.L. Arnal, A.T. Lorenzo, Crystallization in nano-confined polymeric systems, in: E. Piorkowska, G. Rutledge (Eds.), *Handbook of Polymer Crystallization*, Wiley, New York, 2013.
- [8] B. Nadan, J. Hsy, H. Chen, *Polym. Rev.* 46 (2006) 143–172.
- [9] H. Takeshita, T. Shiomi, K. Takenaka, F. Arai, *Polymer* 54 (2013) 4776–4789.
- [10] R.M. Michell, I. Blaszczyk-Lezak, C. Mijangos, A.J. Müller, *J. Polym. Sci. Part B: Polym. Phys.* 52 (2014) 1179–1194.
- [11] R.M. Michell, I. Blaszczyk-Lezak, C. Mijangos, A.J. Müller, *J. Polym. Sci. Part B: Polym. Phys.* 52 (2014) 1179–1194.
- [12] P. Dobryyal, H. Xiang, M. Kazuy, T.P. Russell, *Macromolecules* 42 (2009) 9082–9088.
- [13] Y. Sun, M. Steinhart, D. Zschech, R. Adhikari, G.H. Michler, U. Gösele, *Macromol. Rapid. Commun.* 26 (2005) 369–375.
- [14] H. Xiang, K. Shin, T. Kim, S.I. Moon, T.J. McCarthy, T.P. Russell, *Macromolecules* 38 (2005) 1055–1056.
- [15] G.J.A. Sevink, A.V. Zvelindovsky, *J. Chem. Phys.* 128 (2008) 084901.
- [16] Q. Wang, *J. Chem. Phys.* 126 (2007) 024903.
- [17] B. Yu, Q. Jin, D. Ding, B. Li, A.-C. Shi, *Macromolecules* 41 (2008) 4042–4054.
- [18] Y. Zhu, W. Jiang, *Macromolecules* 40 (2007) 2872–2881.
- [19] P. Maniadis, I.N. Tsimpanogiannis, E.M. Kober, T. Lookman, *EPL* 81 (2008) 56001.
- [20] R.M. Michell, A.T. Lorenzo, A.J. Müller, M.-C. Lin, I. Blaszczyk-Lezak, J. Martín, C. Mijangos, *Macromolecules* 45 (2012) 1517–1528.
- [21] Y. Suzuki, H. Duran, M. Steinhart, H.J. Butt, G. Floudas, *Macromolecules* 47 (2014) 1793–1800.
- [22] A.T. Lorenzo, M.L. Arnal, A.J. Müller, A. Boschetti de Fierro, V. Abetz, *Eur. Polym. J.* 42 (2006) 516–533.
- [23] A.J. Müller, A.T. Lorenzo, R.V. Castillo, M.L. Arnal, A. Boschetti-de-Fierro, V. Abetz, *Macromol. Symp.* 245–246 (2006) 154–160.
- [24] A.J. Müller, A.T. Lorenzo, M.L. Arnal, A. Boschetti de Fierro, V. Abetz, *Macromol. Symp.* 240 (2006) 114–122.
- [25] A.T. Lorenzo, M.L. Arnal, A.J. Müller, A. Boschetti-de-Fierro, V. Abetz, *Macromolecules* 40 (2007) 5023–5037.
- [26] A.P. Li, F. Müller, A. Birner, K. Nielsch, U. Gosele, *J. Appl. Phys.* 84 (1998) 6023–6026.
- [27] H. Masuda, K. Fukuda, *Science* 268 (1995) 1466–1468.
- [28] V. Mathot, *Calorimetry and Thermal Analysis of Polymers*, Hanser Publishers, New York, 1994.
- [29] A.J. Müller, V. Balsamo, M.L. Arnal, T. Jakob, H. Schmalz, V. Abetz, *Macromolecules* 35 (2002) 3048–3058.
- [30] J.L. Carvalho, K. Dalnoki-Veress, *Eur. Phys. J. E.* 34 (2011) 1–6.
- [31] J.L. Carvalho, K. Dalnoki-Veress, *Phys. Rev. Lett.* 105 (2010) 237801.